

## Multifractality and Conformal Invariance at 2D Metal-Insulator Transition in the Spin-Orbit Symmetry Class

H. Obuse,<sup>1</sup> A. R. Subramaniam,<sup>2,3</sup> A. Furusaki,<sup>1</sup> I. A. Gruzberg,<sup>2,3</sup> and A. W. W. Ludwig<sup>3,4</sup>

<sup>1</sup>Condensed Matter Theory Laboratory, RIKEN, Wako, Saitama 351-0198, Japan

<sup>2</sup>James Franck Institute, University of Chicago, 5640 South Ellis Avenue, Chicago, Illinois 60637, USA

<sup>3</sup>Kavli Institute for Theoretical Physics, University of California, Santa Barbara, California 93106, USA

<sup>4</sup>Physics Department, University of California, Santa Barbara, California 93106, USA

(Received 22 September 2006; published 12 April 2007)

We study the multifractality (MF) of critical wave functions at boundaries and corners at the metal-insulator transition (MIT) for noninteracting electrons in the two-dimensional (2D) spin-orbit (symplectic) universality class. We find that the MF exponents near a boundary are different from those in the bulk. The exponents at a corner are found to be directly related to those at a straight boundary through a relation arising from conformal invariance. This provides direct numerical evidence for conformal invariance at the 2D spin-orbit MIT. The presence of boundaries modifies the MF of the whole sample even in the thermodynamic limit.

DOI: 10.1103/PhysRevLett.98.156802

PACS numbers: 73.20.Fz, 05.45.Df, 72.15.Rn

Anderson metal-insulator transitions (MITs), i.e., localization-delocalization transitions of noninteracting electrons, are continuous phase transitions driven by disorder. At the transition, wave functions (WFs) are neither localized nor simply extended, but are complicated scale invariant fractals exhibiting multifractal behavior characterized by a continuous set of scaling exponents [1–4]. In two dimensions the universal critical properties at a host of conventional phase transitions are known to be described by conformal field theories (CFTs) [5]. It is natural to expect that disorder-averaged observables at a localization transition in 2D are also governed by a CFT. If so, then conformal symmetry should impose severe constraints on averages of local quantities, including moments of WF amplitudes.

In a recent Letter, Subramaniam *et al.* [6] extended the notion of multifractality (MF) to the boundaries of the sample (“surface MF”), and showed that near boundaries critical WFs are characterized by MF exponents that are different from those in the bulk. Moreover, it was predicted that the MF of the entire system depends crucially on the presence or absence of boundaries, even in the thermodynamic limit. In this Letter we study surface MF at the MIT in 2D for noninteracting electrons with spin-orbit scattering (symplectic universality class) [7], and extend the surface MF analysis to boundaries with corners (“corner MF”). Conformal symmetry, if present, would lead (following [8]) to a simple exact prediction relating corner and surface MF exponents. Here, we show numerically that at the 2D spin-orbit MIT this prediction is indeed valid, thereby providing direct evidence for the presence of conformal symmetry at this MIT. We also confirm the dependence of the MF of the whole system on the presence of boundaries, as predicted in [6].

We begin by introducing corner and surface MF [6,9] for a rhombus [Fig. 1(a)] and a cylinder [Fig. 1(b)], both having edges of length  $L$ . All WFs  $\psi(\mathbf{r})$  vanish at the

boundaries. We define the corner ( $\theta$ ) with opening angle  $\theta$ , surface ( $s$ ), and bulk ( $b$ ) regions of the rhombus, and similar regions  $s$ ,  $b$  of the cylinder, as illustrated in Fig. 1. In each region  $\theta$ ,  $s$ , or  $b$ , the MF of WFs is characterized by the scaling of the moments of  $|\psi(\mathbf{r})|^2$  with the system size  $L$  [all WFs  $\psi(\mathbf{r})$  are normalized],

$$L^{d_x} \overline{|\psi(\mathbf{r})|^{2q}} \sim L^{-\tau_q^x}, \quad (x = \theta, s, b, w), \quad (1)$$

where  $d_x$  is the spatial dimension of each region ( $d_b = 2$ ,  $d_s = 1$ , and  $d_\theta = 0$ ). The overbar represents the ensemble (disorder) average and the simultaneous spatial average over a region  $x$  surrounding the point  $\mathbf{r}$ .  $\tau_q^b$ ,  $\tau_q^s$ , and  $\tau_q^\theta$  are the bulk, surface, and corner MF exponents, respectively. By  $x = w$  we label quantities computed by spatially averaging over the whole system ( $d_w = 2$ ) [6].

Nonvanishing anomalous dimensions  $\Delta_q^x$ ,

$$\Delta_q^x \equiv \tau_q^x - 2q + d_x, \quad (2)$$

distinguish a critical point from a simple metallic phase in which  $\Delta_q^x \equiv 0$ . By the definition (1) and (2),  $\Delta_q^x$  vanish at  $q = 0$  and 1. The exponent  $\mu$  defined in [6] is absent in Eq. (2) because the local density of states is independent of energy at the spin-orbit MIT. The MF singularity spectra  $f^x(\alpha)$  are obtained from  $\tau_q^x$  by Legendre transformation,

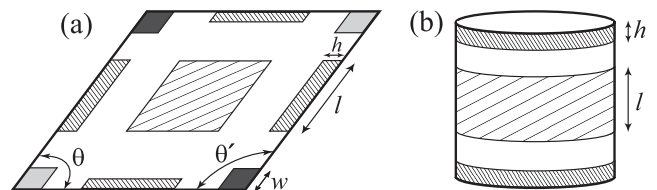


FIG. 1. Systems studied: (a) A rhombus with the bulk, surface, and corner regions of sizes  $l \times l$ ,  $l \times h$ , and  $w \times w$  sites, correspondingly; (b) a cylinder with the bulk ( $L \times l$ ) and surface ( $L \times h$ ) regions.

$$f^x(\alpha^x) = \alpha^x q - \tau_q^x, \quad \alpha^x = d\tau_q^x/dq. \quad (3)$$

$f^x(\alpha)$  have the meaning of fractal dimensions: the number of points  $\mathbf{r} \in x$ , where  $|\psi(\mathbf{r})|^2$  scales as  $L^{-\alpha}$ , is proportional to  $L^{f^x(\alpha)}$ . This gives a direct relation between  $f^x(\alpha)$  and the distribution functions of WF amplitudes:

$$P_x(|\psi|^2) \sim |\psi|^{-2} L^{f^x(\alpha) - d_x}, \quad \alpha = -\ln|\psi|^2/\ln L. \quad (4)$$

Since  $f^\theta(\alpha^\theta) \leq d_\theta = 0$ , the ensemble average is essential [10] for defining corner MF.

Suppose that the  $q$ th moment  $\overline{|\psi(\mathbf{r})|^{2q}}$  is represented by a local operator in an underlying critical field theory describing disorder averages. The scaling dimension of this operator will then equal  $\Delta_q$  [11]. If the field theory possesses conformal invariance and if the operator is (Virasoro) primary, then the relation  $\Delta_q^\theta = \frac{\pi}{\theta} \Delta_q^s$  between the surface and corner exponents can be derived [8] from the conformal mapping  $w = z^{\theta/\pi}$ . This yields

$$\alpha_q^\theta - 2 = \frac{\pi}{\theta}(\alpha_q^s - 2), \quad f^\theta(\alpha_q^\theta) = \frac{\pi}{\theta}[f^s(\alpha_q^s) - 1]. \quad (5)$$

The validity of these relations provides direct evidence for conformal invariance at a 2D localization critical point, and for the primary nature of this operator. We note, however, that Eqs. (5) are valid only if  $\alpha_q^\theta > 0$ , because  $\alpha$  is non-negative for normalized WFs [3,4]. It is expected [10] that for  $q > q_\theta$  (where  $q_\theta$  is a solution to  $\alpha_q^\theta = 0$ ) the exponents  $\tau_q^\theta$  become independent of  $q$ , while  $\alpha_q^\theta = 0$  [Eq. (3)]. With the definition (2) this leads to a modified relation between  $\Delta_q^\theta$  and  $\Delta_q^s$ :

$$\Delta_q^\theta = \begin{cases} \frac{\pi}{\theta} \Delta_q^s, & q < q_\theta, \\ \frac{\pi}{\theta} \Delta_{q_\theta}^s - 2(q - q_\theta), & q > q_\theta. \end{cases} \quad (6)$$

In [6] it was argued that when the MF in the whole sample with a smooth boundary is analyzed, the lowest of the  $\tau_q$  exponents for bulk and boundary dominates:  $\tau_q^v = \min(\tau_q^b, \tau_q^s)$ . Points where the curves  $\tau_q^b$  and  $\tau_q^s$  intersect translate into linear segments on the plot of  $f^w(\alpha)$  (necessarily convex), interpolating between  $f^b(\alpha)$  and  $f^s(\alpha)$ , see Fig. 3 in [6].

In a recent Letter, Mirlin *et al.* pointed out that  $\Delta_q^b$  obey the relation  $\Delta_q^b = \Delta_{1-q}^b$ , which is expected to hold also for surface MF [12]. In two dimensions this leads to

$$f^x(\alpha_{1-q}^x) - \frac{\alpha_{1-q}^x}{2} = f^x(\alpha_q^x) - \frac{\alpha_q^x}{2}, \quad \alpha_{1-q}^x = 4 - \alpha_q^x, \quad (7)$$

and implies that  $\alpha^x$  cannot exceed 4.

To test all these theoretical predictions for the 2D spin-orbit MIT, we employ the ‘‘SU(2) model’’ defined in [13], which is a tight-binding model on a 2D square lattice with on-site disorder and a random SU(2) nearest-neighbor hopping. We consider four different lattice geometries: (i) *torus*, i.e., a square lattice with periodic boundary conditions (PBC) imposed in the  $x$  and  $y$  directions, (ii) *cylinder* [Fig. 1(b)] with PBC imposed in the  $x$  direc-

tion and open boundary conditions (OBC) in the  $y$  direction, (iii) *square* with OBC in the  $x$  and  $y$  directions, and (iv) *rhombus* [Fig. 1(a)] with  $\theta = \pi/4$  and  $\theta' = 3\pi/4$  and OBC imposed in the  $x$  and  $y$  directions. In all these geometries the number of lattice sites is  $L^2$ .

For the scaling analysis the system size  $L$  is varied through  $L = 24, 30, 36, \dots, 120$ . For a fixed on-site disorder strength  $W_c$ , we examined  $6 \times 10^4$  samples with different disorder configurations for each  $L$ . We have used the forced oscillator method [14] to diagonalize the Hamiltonian, and extracted one critical WF from each sample which had the energy eigenvalue closest to the critical energy  $E_c = 1$  at  $W_c = 5.952$  (in the unit of hopping strength). For the results presented below, we have set  $l = L/6$ ,  $h = 1$  for the cylinders [Fig. 1(b)], and  $w = 4$  for the corners [Fig. 1(a)]. We have numerically confirmed that the exponents computed in the bulk regions of rhombi and cylinders agree with those of tori within statistical error bars. Also, the MF exponents for the surface region of rhombi are, within error bars, equal to those computed for the surface region of cylinders. In the following figures the bulk (surface) exponents are those computed for tori (for the surface region of cylinders).

Figure 2 shows the probability distribution functions (PDFs) of  $\ln|\psi(\mathbf{r})|^2$  measured for  $\mathbf{r}$  at corners with angle  $\theta = \pi/4$  (light blue) and  $\theta = \pi/2$  (pink), at the boundary of cylinders (blue), and in the bulk region of cylinders (black) at the fixed  $L = 120$ . Each PDF is normalized in the region where it is defined. The PDF calculated for tori is also shown in red, and it agrees quantitatively with the bulk PDF (black), as expected. Clearly, the PDFs for bulk, surface, and corner with  $\theta = \pi/2$  and  $\theta = \pi/4$ , are all different, and, in this order, the peak position is shifted to the left, in agreement with the expectation that WF amplitudes should be smaller near edges. In the same order, the distributions become broader with longer (presumably power-law) tails at  $|\psi|^2 L^2 \gg 1$ . This means that for large  $q$  the moments  $\overline{|\psi(\mathbf{r})|^{2q}}$  can become larger near edges

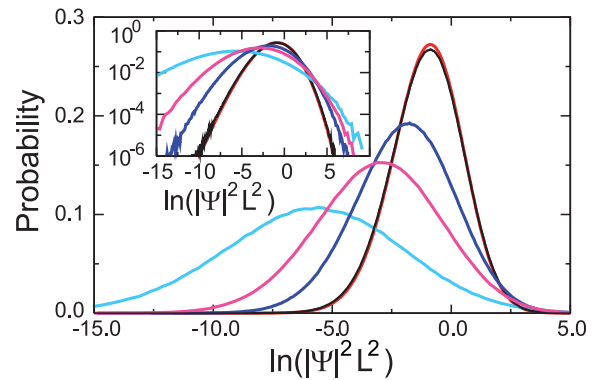


FIG. 2 (color). PDFs of logarithm of WF amplitudes on tori (red), in the bulk region of cylinders (black), in the surface region of cylinders (blue), and in the corner region with  $\theta = \pi/2$  (pink) and  $\theta = \pi/4$  (light blue);  $L = 120$ . Inset: Semi-logarithmic plot.

(corners) than in the bulk, as the higher moments are dominated by long tails [10].

We numerically obtain  $\alpha_q^x$  and  $f^x(\alpha_q^x)$  from [see (1) and (3)]

$$\langle\langle \ln|\psi|^2 \rangle\rangle_q \equiv \frac{|\overline{|\psi(\mathbf{r})|^{2q} \ln|\psi(\mathbf{r})|^2}}{|\overline{|\psi(\mathbf{r})|^{2q}}} \sim -\alpha_q^x \ln L, \quad (8)$$

$$\overline{|\psi(\mathbf{r})|^{2q}} \sim [f^x(\alpha_q^x) - \alpha_q^x q - d_x] \ln L. \quad (9)$$

The inset of Fig. 3(a) shows  $\langle\langle \ln|\psi|^2 \rangle\rangle_q$  as functions of  $L$ , computed for tori ( $x = b$ ), at the boundary of cylinders ( $x = s$ ), and at the corners ( $\theta = \pi/2$ ) of squares. This inset exhibits distinct scaling behavior for bulk, surface, and corner regions for the displayed values of  $q = 1, 3$ .

Figure 3(a) shows  $f^x(\alpha)$  of the bulk, surface, and corner ( $\theta = \pi/2$ ) regions. Clearly, in this order, the spectra  $f^x(\alpha)$  are seen to become broader and their maxima  $\alpha_0^x$  are shifted to the right ( $\alpha_0^b = 2.173 \pm 0.001$ ,  $\alpha_0^s = 2.417 \pm 0.002$ ,  $\alpha_0^{\pi/2} = 2.837 \pm 0.003$ ), in accordance with Fig. 2 and Eq. (4). [Recall that the maximal values of  $f^x(\alpha)$  are

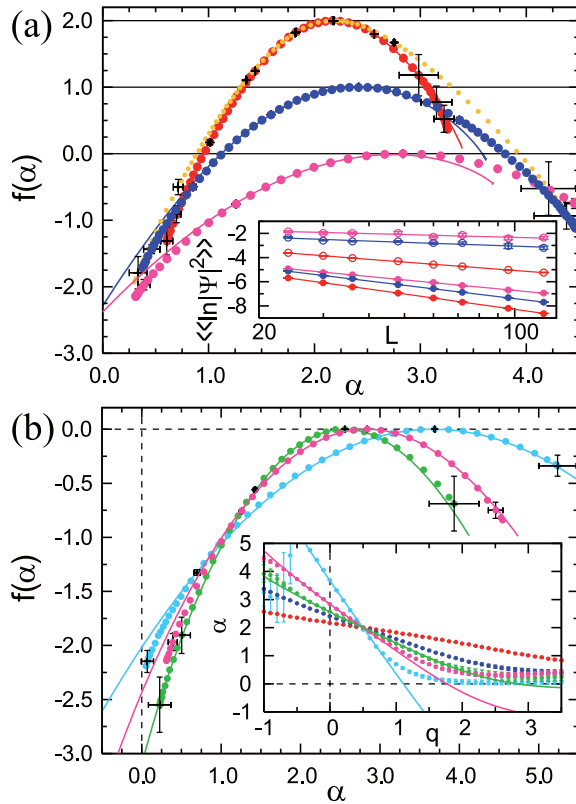


FIG. 3 (color). (a) Bulk (red), surface (blue), corner  $\theta = \pi/2$  (pink), and whole cylinder (orange)  $f(\alpha)$  spectra, with error bars shown at integer values of  $q$ . Red, blue, and pink curves represent  $f^x(4 - \alpha) + \alpha - 2$ . Inset: Scaling plot of Eq. (8) at  $q = 1$  (filled circles) and  $q = 3$  (open circles). (b) Corner  $f(\alpha)$  spectra at  $\theta = \pi/4$  (light blue),  $\pi/2$  (pink), and  $3\pi/4$  (green), with error bars shown at integer  $q$  (and at  $q = -0.5$  for  $\theta = \pi/4$ ). Curves represent the conformal relation (5). Inset: Numerical results for  $\alpha_q^x$  compared with Eqs. (5) (colored curves).

the spatial dimensions  $d_x$ .] The plot of  $f^w(\alpha)$  for the whole cylinder [Fig. 3(a), orange] clearly represents the convex hull of  $f^b(\alpha)$  and  $f^s(\alpha)$  [6,15]. Notice that  $f^w(\alpha)$  deviates from  $f^b(\alpha)$  already at  $f(\alpha) \approx 1.5$  (for  $q < 0$ ). This confirms the prediction of [6] that the presence of boundaries drastically affects the MF of the system even in the thermodynamic limit and also in a typical sample [where  $f(\alpha) \geq 0$  [10]].

The data points of the bulk spectrum  $f^b(\alpha)$  [red dots in Fig. 3(a)] lie on top of the red curve representing data points [16] for  $f^b(\alpha_{1-q}^b)$  in Eq. (7). This confirms Eq. (7) for the bulk which is the consequence of the symmetry relation [12]. Incidentally, the value of the typical bulk exponent  $\alpha_0^b$  agrees with earlier calculations [17,18] but not with [19]. Furthermore, our  $\alpha_0^b$  satisfies  $\pi(\alpha_0^b - 2) = 1/\Lambda_c$  [3], where  $\Lambda_c = 1.843$  is the quasi-1D localization length at the MIT, normalized by the wire width, as obtained in [13]. The surface spectrum  $f^s(\alpha)$  (blue) is also seen to satisfy the relation (7) for  $1 \leq \alpha^s \leq 3$ , but there are discrepancies between the blue dots and the curve  $f^s(\alpha_{1-q}^s)$  when  $\alpha_q^s > 3$  ( $q < -0.7$ ) and  $\alpha_q^s < 1$  ( $q > 2$ ). Moreover, it appears that  $\alpha_q^s$  can exceed 4, in contrast to  $\alpha_q^b < 4$ . This may question the validity of the symmetry relation of [12] for boundaries, but we feel that computations on even larger system sizes and numbers of samples are necessary for drawing a definite conclusion.

Figure 3(b) shows the corner spectra  $f^\theta(\alpha)$  at  $\theta = 3\pi/4$  (green),  $\pi/2$  (pink), and  $\pi/4$  (light blue). As  $\theta$  decreases, the peak position moves to the right ( $\alpha_0^{3\pi/4} = 2.558 \pm 0.003$ ,  $\alpha_0^{\pi/2} = 2.837 \pm 0.003$ , and  $\alpha_0^{\pi/4} = 3.689 \pm 0.006$ ) and the spectra become broader, indicating that at smaller  $\theta$  the typical value of a WF amplitude is smaller but its distribution is broader. The numerical data (dots) are compared with the curves predicted from conformal invariance, Eq. (5), using  $f^s(\alpha^s)$  of Fig. 3(a) within the range  $1 \leq \alpha^s \leq 3$ , where  $|q|$  is sufficiently small to ensure good numerical accuracy. The agreement between the numerical data and the predicted curves is excellent, confirming the presence of conformal symmetry.

The inset of Fig. 3(b) shows  $\alpha_q^x$  where the curves represent  $\alpha_q^x$  computed with  $\alpha_q^s$  as input in Eq. (5). Note that  $\alpha^x = 2$  at  $q = 1/2$  as a consequence of Eq. (7). We see that the numerical data for  $\alpha_q^x$  deviate from the predicted curves, Eq. (5), when  $\alpha_q^x \leq 1$ , in order to satisfy the constraint  $\alpha_q^x > 0$ . We expect that in the limit  $L \rightarrow \infty$ ,  $\alpha_q^x$  be given by Eq. (5) for  $q < q_\theta$  and by  $\alpha_q^x = 0$  for  $q > q_\theta$ .

We note that the numerical results for  $\alpha_q^x$  exceed 4 when  $q \leq -0.1$  for  $\theta = \pi/4$ , and  $q \leq -0.7$  for  $\theta = \pi/2$  [Fig. 3(b) and inset]. Even the maximum  $\alpha_0^\theta$  of  $f^\theta(\alpha)$  will exceed 4 for sufficiently small angles  $\theta$ . On one hand, the maximum corresponds to  $q = 0$  where the numerics are most accurate. On the other hand, the maximal value  $f^\theta(\alpha) = d_\theta = 0$  has a direct physical meaning as the dimension of the WF support, and must therefore appear on the  $f^\theta(\alpha)$  curve. Thus, our data strongly indicate that the symmetry relation of [12] is violated for corners.

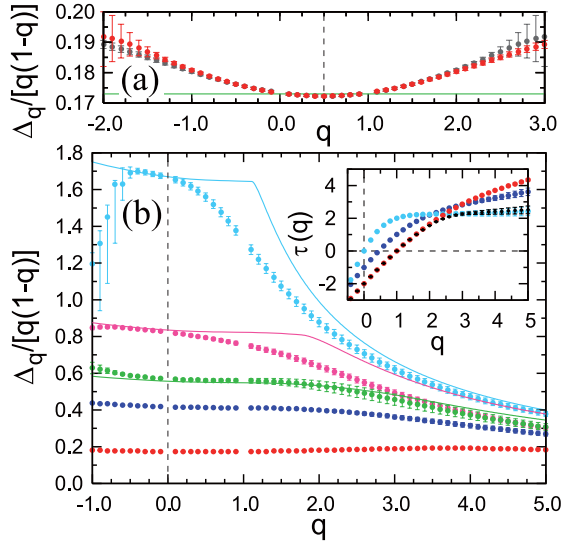


FIG. 4 (color). (a) The numerical data for the bulk exponents  $\Delta_q^b$  (red) are compared with their mirror image  $\Delta_{1-q}^b$  (gray). The green line represents  $\alpha_0^b - 2$ . (b) The exponents  $\Delta_q/[q(1-q)]$  for the bulk (red), the surface (blue), and corners with  $\theta = \pi/4$  (light blue),  $\pi/2$  (pink), and  $3\pi/4$  (green). The curves represent the theoretical prediction, Eq. (6). Inset: Bulk (red), surface (blue), and corner ( $\theta = \pi/4$ , light blue) exponents  $\tau_q^x$ , and  $\tau_q^w$  for a whole rhombus with  $\theta = \pi/4$  (black).

The anomalous dimensions  $\Delta_q^x$  are computed numerically from  $|\psi(\mathbf{r})|^{2q}/(|\psi(\mathbf{r})|^2)^q \sim L^{-\Delta_q^x}$ , which follows from Eqs. (1) and (2). Figure 4(a) shows the bulk anomalous dimension  $\Delta_q^b$  (red) and its mirror image across the  $q = 1/2$  line  $\Delta_{1-q}^b$  (gray), both rescaled by  $q(1-q)$ . Note that this rescaling magnifies small numerical errors around  $q = 0$  and  $q = 1$ . Nevertheless, the numerical data satisfy the relation  $\Delta_q^b = \Delta_{1-q}^b$  of [12] for  $-1 < q < 2$  where statistical errors are small. It is also clear from Fig. 4(a) that  $\Delta_q^b/[q(1-q)]$  varies with  $q$ , which means that the bulk spectrum  $f^b(\alpha)$  is not exactly parabolic.

Figure 4(b) compares  $\Delta_q^x$  for bulk, surface, and corners with  $\theta = \pi/4, \pi/2$ , and  $3\pi/4$ . The solid curves represent the theoretical prediction (6) from the conformal mapping, where  $\Delta_q^s$  is taken from Fig. 4(b). For sufficiently small values of  $|q|$  the numerical results of  $\Delta_q^\theta$  are in good quantitative agreement with the prediction (6). It is precisely for small  $|q|$  that the numerical data are most accurate [20]. This provides direct evidence for the presence of conformal symmetry at the 2D spin-orbit MIT.

The inset of Fig. 4(b) shows the exponents  $\tau_q^x$  for bulk, surface, and corners. We see that  $\tau_q^{\pi/4}$  (light blue) is constant for  $q > q_{\pi/4} \approx 1$  reflecting the exchange between top and bottom lines in Eq. (6) which happens at  $\alpha_q^{\pi/4} = 0$ . It appears that  $\tau_q^{\pi/4}$  becomes smaller than both  $\tau_q^s$  and  $\tau_q^b$  for  $q \gtrsim 2.5$ , which is when the corner exponent  $\tau_q^{\pi/4}$  controls the MF of the whole sample with a  $\pi/4$  corner, as shown in black. In a sample without corners such as a

cylinder, the surface exponent  $\tau_q^s$  controls the MF of the entire sample for sufficiently large  $q$ . This confirms and generalizes the predictions made in [6].

In summary, we studied bulk, surface, and corner multifractality at the MIT in the 2D spin-orbit symmetry class. We provided direct numerical evidence for the presence of conformal symmetry at this critical point, and confirmed predictions of [6] that boundaries affect MF of the whole system even in the thermodynamic limit. We also tested the validity of the symmetry relation of [12] for the bulk, surface, and corners. It appears that the relation holds in the bulk, but is violated at corners.

We thank A. Mirlin for discussions. This work was supported by NAREGI Grant from MEXT of Japan, the NSF under Grant No. PHY99-07949, the NSF MRSEC under No. DMR-0213745, the NSF Career Grant No. DMR-0448820, the Alfred P. Sloan Foundation, and Research Corporation. Numerical calculations were performed on the RIKEN Super Combined Cluster System.

*Note added.*—Recent numerical work on the bulk MF in the 2D symplectic class [21] agrees with our results for the bulk.

- [1] F. Wegner, Z. Phys. B **36**, 209 (1980).
- [2] C. Castellani and L. Peliti, J. Phys. A **19**, L429 (1986).
- [3] M. Janssen, Phys. Rep. **295**, 1 (1998).
- [4] A. D. Mirlin, Phys. Rep. **326**, 259 (2000).
- [5] A. A. Belavin, A. M. Polyakov, and A. B. Zamolodchikov, Nucl. Phys. **B241**, 333 (1984).
- [6] A. R. Subramaniam *et al.*, Phys. Rev. Lett. **96**, 126802 (2006).
- [7] S. Hikami, A. I. Larkin, and Y. Nagaoka, Prog. Theor. Phys. **63**, 707 (1980).
- [8] J. L. Cardy, Nucl. Phys. **B240**, 514 (1984).
- [9] A. R. Subramaniam *et al.* (unpublished).
- [10] F. Evers and A. D. Mirlin, Phys. Rev. Lett. **84**, 3690 (2000); A. D. Mirlin and F. Evers, Phys. Rev. B **62**, 7920 (2000).
- [11] B. Duplantier and A. W. W. Ludwig, Phys. Rev. Lett. **66**, 247 (1991).
- [12] A. D. Mirlin *et al.*, Phys. Rev. Lett. **97**, 046803 (2006).
- [13] Y. Asada, K. Slevin, and T. Ohtsuki, Phys. Rev. Lett. **89**, 256601 (2002); Phys. Rev. B **70**, 035115 (2004).
- [14] T. Nakayama and K. Yakubo, Phys. Rep. **349**, 239 (2001).
- [15] The interpolating portions of  $f^w(\alpha)$  are slightly curved due to finite size effects.
- [16] Here the data points are drawn very closely spaced so as to appear to the eye as a continuous curve.
- [17] L. Schweitzer, J. Phys. Condens. Matter **7**, L281 (1995).
- [18] R. Merkt, M. Janssen, and B. Huckestein, Phys. Rev. B **58**, 4394 (1998).
- [19] P. Markos and L. Schweitzer, J. Phys. A **39**, 3221 (2006).
- [20] For  $q \gtrsim 1$ , Fig. 4(b) shows discrepancies between the numerical results and the prediction from CFT, enhanced by the  $(1-q)^{-1}$  factor. In this range of  $q$  the moments of  $|\psi|^2$  are dominated by rare events, which makes it difficult to obtain accurate numerical data.
- [21] A. Mildenerger and F. Evers, Phys. Rev. B **75**, 041303(R) (2007).